Preferential Sampling and Small-Scale Clustering of Gyrotactic Microswimmers in Turbulence

K. Gustavsson,[1,2] F. Berglund,[1] P. R. Jonsson,[3] and B. Mehlig[1]
[1]Department of Physics, Gothenburg University, SE-41296 Gothenburg, Sweden
[2]Department of Physics and INFN, University of Rome 'Tor Vergata', 00133 Rome, Italy
[3]Department of Biological and Environmental Sciences—Tjärnö, SE-45296 Strömstad, Sweden
(Received 10 January 2015; revised manuscript received 15 January 2016; published 10 March 2016)

Recent studies show that spherical motile microorganisms in turbulence subject to gravitational torques gather in down-welling regions of the turbulent flow. By analyzing a statistical model we analytically compute how shape affects the dynamics, preferential sampling, and small-scale spatial clustering. We find that oblong organisms may spend more time in up-welling regions of the flow, and that all organisms are biased to regions of positive fluid-velocity gradients in the upward direction. We analyze small-scale spatial clustering and find that oblong particles may either cluster more or less than spherical ones, depending on the strength of the gravitational torques.

DOI: 10.1103/PhysRevLett.116.108104

Patchiness in suspensions of microorganisms is frequently observed on a range of spatial scales. The underlying mechanisms differ, depending on the properties of the microorganisms, and upon the spatial scale. Patchiness can be caused by density stratification and vertical shears [1], by predator-prey cycles, or by interactions between the organisms and water-column gradients—in light, chemistry, turbulence, and in hydrostatic pressure [2]. Patchiness is important because many biological processes (mating, feeding, predation) rely on individual encounters [3], and the encounter rate is strongly influenced by small-scale number-density fluctuations.

Gravitaxis may cause such inhomogeneities in the spatial distribution of motile microorganisms. Density or drag asymmetries of the body give rise to torques affecting the swimming direction [4–6]. When the effects of gyrotactic torques and fluid-velocity gradients balance, inhomogeneities may form in the spatial distribution, as shown by the microalgae *Chlamydomonas nivalis* swimming up against a down-welling pipe flow. The microalgae gather in the center of the pipe where the down-welling velocity is largest [7]. Gyrotaxis may trap motile organisms in macroscopic shear gradients [8,9], and fluctuating vorticity may cause patchiness [10]. This is confirmed by recent direct numerical simulations (DNS) of motile, spherical microorganisms in turbulence [11] revealing that the organisms are more likely to be found in down-welling regions of the turbulent flow; they "preferentially sample" such regions.

These results raise three fundamental questions that we address and answer in this Letter. First, how does shape affect the dynamics in turbulence of motile microorganisms subject to gyrotaxis? In Ref. [11] the organisms were assumed to be spherical. Nonspherical organisms respond not only to turbulent vorticity but also to turbulent strain [12–15]. This causes passive rods to exhibit intricate orientational patterns on the surface of turbulent and other complex flows [16–18]. Also, shape strongly affects the trajectories of active particles in model flows [19–21], and recent DNS indicate that prolate gyrotactic organisms cluster less than spherical ones when gyrotaxis is strong [22]. Second, where do the organisms go in turbulence? Are there circumstances where the organisms may not gather in down-welling regions, or where other mechanisms of preferential sampling may apply? Third, the fact that orgamisms tend to gather in certain regions of the flow (preferential sampling) does not explain which mechanisms actually cause them to get in contact. To determine these one must follow the dynamics of two organisms that are initially very close together, and determine whether they tend to approach further or move apart. We refer to the resulting small-scale spatial fluctuations in the number density as "small-scale clustering".

Statistical model.—To answer these questions we use a simplified model [7,11,22] for the translation and rotation of small axisymmetric active particles subject to turbulence and gyrotaxis:

$$\dot{\boldsymbol{r}} \equiv \boldsymbol{v} = \boldsymbol{u}(\boldsymbol{r},t) + v_s\boldsymbol{n} \quad \text{and} \quad \dot{\boldsymbol{n}} = \boldsymbol{\omega}(\boldsymbol{r},t) \wedge \boldsymbol{n}. \quad (1)$$

Dots denote derivatives with respect to time t, $\boldsymbol{r}$ is the particle position, and $\boldsymbol{u}$ is the flow velocity. Each particle swims with constant speed v_s in the direction $\boldsymbol{n}$ of its symmetry axis ($|\boldsymbol{n}| = 1$). The angular velocity of the particle is

$$\boldsymbol{\omega}(\boldsymbol{r},t) = (\hat{\boldsymbol{g}} \wedge \boldsymbol{n})/(2\mathcal{B}) + \Omega(\boldsymbol{r},t) + \Lambda\boldsymbol{n} \wedge [\mathbb{S}(\boldsymbol{r},t)\boldsymbol{n}]. \quad (2)$$

The first term on the right-hand side describes gyrotaxis. The unit vector $\hat{\boldsymbol{g}}$ points in the direction $-\boldsymbol{e}_z$ of gravity, and $\mathcal{B}$ is the reorientation time [7,11]. It depends on the mass distribution within the particle, and on its shape through hydrodynamic resistance. The other terms on the right-hand

side of Eq. (2) represent the effect of the turbulent velocity gradients upon the particle orientation [12]: $\Omega = (\nabla \wedge \boldsymbol{u})/2$, and $\mathbb{S}$ is the symmetric part of the matrix $\mathbb{A}$ of fluid-velocity gradients. The parameter Λ characterizes particle shape: $\Lambda = 0$ for spheres, and $\Lambda = 1$ for infinitely thin rods. Equation (2) disregards turbulent accelerations. In most marine conditions this is an excellent approximation [23]. We model the dissipative range of turbulence by incompressible, homogeneous, isotropic Gaussian random functions with typical length, time, and speed scales η, τ, u_0 [24]. This neglects inertial-range properties which may become important for particles that are larger than the Kolmogorov length [25]. We note that the dissipative-range turbulent fluctuations are universal [26], but they are not Gaussian. We comment on this difference between turbulence and the statistical model below.

There are four dimensionless parameters: the shape parameter Λ, the reorientation time $\Psi = \mathcal{B}/\tau$, the swimming speed $\Phi = v_s\tau/\eta$, and the Kubo number $\mathrm{Ku} = u_0\tau/\eta$. We vary the parameters independently, keeping $\mathcal{B}$ constant as Λ is changed. Ku is a dimensionless measure of the correlation time of the flow.

Our choice of the dimensionless parameters is dictated by the method (explained below). DNS employ different dedimensionalizations [11]: $\mathcal{B}$ by the Kolmogorov time $\tau_K \equiv 1/\sqrt{\mathrm{Tr}\langle \mathbb{A}\mathbb{A}^T\rangle_\infty}$, and v_s by the corresponding Kolmogorov speed u_K. Our dimensionless parameters translate to those used in the DNS as $\Psi_{\mathrm{DNS}} \sim \mathrm{Ku}\Psi$ and $\Phi_{\mathrm{DNS}} \sim \Phi/\mathrm{Ku}$. We expect that the statistical-model results become independent of Ku at large Ku and qualitatively agree with DNS results [24].

Typical values of $\mathcal{B}$, v_s are given in Ref. [5]: $\mathcal{B} \sim 1$–5 s and $v_s \sim 0.1$–1 mm/s. Typical ocean dissipation rates are $\varepsilon \sim 1$–10^2 mm^2/s^3 for surface water [27], giving Kolmogorov times, lengths, and speeds in the range $\tau_K \sim 0.1$–1 s, $\eta \sim 0.3$–1 mm, and $u_K \sim 1$–3 mm/s. These estimates yield $\Psi_{\mathrm{DNS}} \sim 1$–$50$ and $\Phi_{\mathrm{DNS}} \sim 0.03$–$1$. In Ref. [28] smaller dissipation rates, $\varepsilon \sim 10^{-4}$ mm^2/s^3, are quoted for the very deep sea. This extends the ranges to $\Psi_{\mathrm{DNS}} \sim 0.01$–$50$ and $\Phi_{\mathrm{DNS}} \sim 0.03$–$10$.

Method.—Equations (1), (2) can be solved by iteratively refining approximations for the path a particle takes through the flow [24,29,30]. This results in expansions of steady-state averages in powers of Ku and allows us to determine how the remaining parameters (Φ, Ψ, and Λ) affect preferential sampling and small-scale clustering. The details of this calculation are given in the Supplemental Material [31]. Here we outline the essential steps. First, to consistently track the orders in the expansion we dedimensionalize $t' = t/\tau, \boldsymbol{r}' = \boldsymbol{r}/\eta, \boldsymbol{u}' = \boldsymbol{u}/u_0$. Second, we expand the dynamics of the vector $\boldsymbol{n}$ in powers of Ku:

$$\boldsymbol{n}(t') = \sum_{q=0}^{\infty} \boldsymbol{n}_q(t')\mathrm{Ku}^q. \tag{3}$$

Inserting this ansatz into (1), (2) and identifying terms of order Ku^q yields equations for $\boldsymbol{n}_q$ that can be solved in terms of $\boldsymbol{n}_p$ for $p < q$. The lowest-order solution in Ku is just $\boldsymbol{n}_0 = -\hat{\boldsymbol{g}}$. This yields a lowest-order deterministic approximation for the particle position at time t':

$$\boldsymbol{r}'_{\mathrm{det}}(t') = \boldsymbol{r}'_0 - \Phi\hat{\boldsymbol{g}}t'. \tag{4}$$

Third, we expand Eqs. (1), (2) in terms of deviations from the deterministic trajectory $\delta\boldsymbol{r}'(t') \equiv \boldsymbol{r}'(t') - \boldsymbol{r}'_{\mathrm{det}}(t')$ precisely as described in Ref. [24]. In the fourth and final step we average over the fluid-velocity fluctuations in the statistical model. In the remainder of this Letter we summarize the results obtained in this way.

Preferential sampling.—Consider the steady-state averages of the z-component u_z of the fluid velocity and of its gradient, A_{zz}, both evaluated at the particle position. Analytical results for these averages are derived to lowest order in Ku in the Supplemental Material [31], Eqs. (S15) and (S16). These expressions are plotted in Fig. 1. Here we quote only limiting results. For small Φ we have

$$\langle A_{zz}\rangle_\infty \frac{\eta}{u_0} \sim \mathrm{Ku}\Phi^2 \frac{d(1-\Lambda)+2(\Lambda+2)}{d} \frac{\Psi(4\Psi+1)}{(2\Psi+1)^2}, \tag{5a}$$

$$\frac{\langle u_z\rangle_\infty}{u_0} \sim -\mathrm{Ku}\Phi \frac{d(1-\Lambda)+2}{d} \frac{\Psi}{2\Psi+1}, \tag{5b}$$

d is the spatial dimension. For large Φ we find

$$\langle A_{zz}\rangle_\infty \frac{\eta}{u_0} \sim \frac{\mathrm{Ku}}{\Phi} \frac{d+1}{2d}(1-\Lambda)\sqrt{\frac{\pi}{2}}, \tag{6a}$$

$$\frac{\langle u_z\rangle_\infty}{u_0} \sim \frac{\mathrm{Ku}}{\Phi} \frac{[d(\Lambda-1)+2\Lambda]}{2d}. \tag{6b}$$

What can we learn from these analytical results? Equations (5a) and (6a) show that the particles collect in the sinks of the transversal flow-velocity field, $\mathrm{Tr}_\perp\mathbb{A} \equiv -A_{zz} < 0$. This is because gyrotaxis breaks up-down symmetry: when Ψ is small the particles swim essentially upwards (in the $\mathbf{e}_z$ direction), and gather in transversal sinks irrespective of their shape and swimming speed. Simulations [Fig. 1(a)] confirm the theory.

Motivated by Kessler's study in pipe flows [7] the authors of Ref. [11] concluded that spherical particles preferentially sample down-welling regions also in turbulence. This is not in contradiction with the result discussed above because particles may preferentially sample different observables. In fact Eqs. (5b) and (6b) explain that spherical particles are biased towards down-welling regions (as observed in DNS [11]), in addition to sinks in the transversal flow. But (6b) also shows that elongated particles [$\Lambda > d/(d+2)$] preferentially sample up-welling

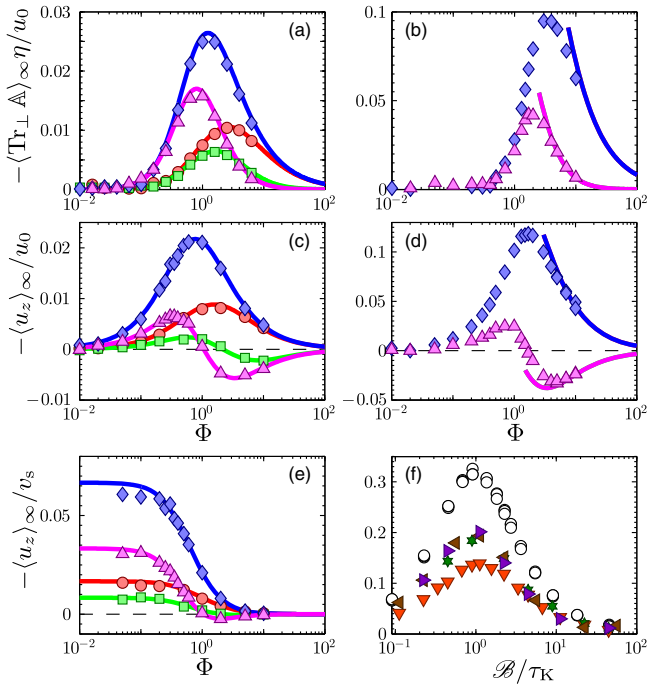

FIG. 1. Preferential sampling. (a) $\langle \mathrm{Tr}_\perp \mathbb{A}\rangle_\infty$ as sampled by the particles. Results of simulations of statistical model: symbols. Eq. (5a): lines. Parameters: $\mathrm{Ku} = 0.1$, $\Psi = 0.1$, $\Lambda = 0$ (red filled circles), $\Psi = 1$, $\Lambda = 0$ (blue filled diamonds), $\Psi = 0.1$, $\Lambda = 1$ (light green filled squares) $\Psi = 1$, $\Lambda = 1$ (pink filled triangles). (b) The same but for $\mathrm{Ku} = 1$ (theory only for large Φ). (c) $\langle u_z\rangle_\infty$ as sampled by the particles for $\mathrm{Ku} = 0.1$. (d) Same but for $\mathrm{Ku} = 1$. (e) $\langle u_z\rangle_\infty/v_s$ as a function of Φ for $\mathrm{Ku} = 0.1$. (f) $\langle u_z\rangle_\infty/v_s$ versus $\mathcal{B}/\tau_K$ for $\Lambda = 0$ and $\mathrm{Ku} = 1$ (red filled triangles), $\mathrm{Ku} = 2$ (dark green filled stars), $\mathrm{Ku} = 5$ (brown filled triangles), $\mathrm{Ku} = 10$ (purple filled triangles). Hollow markers show DNS data from Fig. 3(d) in Ref. [11] (at $\mathrm{Re}_\lambda = 64$). All data are for values of Φ from the small-Φ plateau observed in DNS [11], and also in the statistical model (for $\mathrm{Ku} = 0.1$ this plateau is shown in panel (e), for $\mathrm{Ku} = 1$ in Fig. S1 in the Supplemental Material [31]). Panels (a), (c), (e) are for $d = 2$, panels (b), (d), (f) for $d = 3$.

regions for large enough Φ. This is seen in Fig. 1(c) which shows $\langle u_z\rangle_\infty$ (Eq. (S15) in the Supplemental Material [31]) for $\mathrm{Ku} = 0.1$ and $d = 2$ as a function of Φ. Also shown are results of statistical-model simulations, in excellent agreement with theory. Figure 1(d) shows that the same conclusions hold in three spatial dimensions for $\mathrm{Ku} = 1$. Rods sample upwelling regions when Φ is larger than (approximately) unity.

It is remarkable that the shapes of the curves at $\mathrm{Ku} = 0.1$ are very similar to those at large Ku. This means that the small-Ku theory *qualitatively* explains what is observed in the statistical-model simulations at large Ku and in DNS for spherical particles [11].

In the limit of large Φ particles swim rapidly upwards and experience the flow as a white-noise signal (as in rapid gravitational settling [30]). This limit is universal; particles in *any* homogeneous, isotropic and incompressible flow show preferential sampling according to Eq. (6). This means that the small-Ku theory should describe results of statistical-model simulations at $\mathrm{Ku} = 1$ quantitatively for large Φ. This is confirmed by Figs. 1(b) and 1(d).

For small Φ DNS [11] show that the average of u_z is proportional to Φ for small Φ, so that $\langle u_z\rangle_\infty/\Phi$ is constant. Equation (5b) shows this behavior, in good agreement with simulations [Fig. 1(e)].

We conclude with a quantitative comparison of statistical-model and DNS results [11]. As an example consider the dependence of $\langle u_z\rangle_\infty$ on the reorientation time $\mathcal{B}$. Figure 1(f) shows that the statistical-model result becomes independent of Ku for large Ku, and that it reproduces the DNS results fairly well; it explains the $\mathcal{B}/\tau_K$ dependence of $\langle u_z\rangle_\infty$ of the DNS results up to a prefactor of order unity. This factor is due to the fact that fully developed turbulent velocity fluctuations in the dissipative range differ from those in the statistical model: they are not Gaussian, more persistent, and the probability of straining regions to occur is higher [24].

Small-scale clustering.—Which mechanisms cause two particles caught in the same flow region to actually collide? This is a two-particle problem, only indirectly related to preferential sampling. Fluctuations in the separations between nearby particles are determined by the dynamics of the particle-velocity gradients $\partial v_i/\partial r_j$. Small-scale clustering occurs where $\boldsymbol{\nabla}\cdot\boldsymbol{v} < 0$. We have computed $\langle \boldsymbol{\nabla}\cdot\boldsymbol{v}\rangle_\infty$ to lowest order in Ku. The result is quite lengthy [Eq. (S32) in the Supplemental Material [31]]. For small Φ the full expression simplifies to

$$\langle \boldsymbol{\nabla}\cdot\boldsymbol{v}\rangle_\infty \eta/u_0 \sim -\mathrm{Ku}(\Phi\Psi)^2 B_d(\Lambda) \quad \text{for } \Phi \ll 1, \tag{7}$$

with $B_d(\Lambda) \equiv [(d+2)(d+4) - 2d(d+4)\Lambda + (4+2d+d^2)\Lambda^2]/d$. Since $B_d(\Lambda) > 0$, Eq. (7) implies small-scale clustering. For spherical particles ($\Lambda = 0$) the quadratic dependence of $\langle \boldsymbol{\nabla}\cdot\boldsymbol{v}\rangle_\infty$ on $\Phi\Psi$ was derived in Ref. [11] (and also in Ref. [32]): expanding Eqs. (1), (2) for $\mathcal{B} \ll \tau$ gives

$$\boldsymbol{\nabla}\cdot\boldsymbol{v} \sim v_s\mathcal{B}[-(1+\Lambda)\partial_z^2 u_z + (1-\Lambda)(\partial_z^2 u_z - \Delta u_z)]. \tag{8}$$

Substituting $\Lambda = 0$ yields Eq. (6) of Ref. [11], and averaging Eq. (8) along particle paths results in Eq. (7). The factor $v_s\mathcal{B}$ in (8) corresponds to one factor of $\Phi\Psi$ in (7). The second factor of $\Phi\Psi$ comes from averaging the velocity derivatives in Eq. (8). We note that $\mathrm{Tr}_\perp\mathbb{A}$ does not figure in Eq. (8): preferential sampling of sinks in the flow-velocity field perpendicular to gravity does not contribute to small-scale clustering, showing that the two effects are distinct [24].

Expanding the full result (S32) for large Φ gives

$$\langle \boldsymbol{\nabla}\cdot\boldsymbol{v}\rangle_\infty \eta/u_0 \sim -\mathrm{Ku}\Phi\Psi^2 E_d(\Lambda) \quad \text{for } \Phi \gg 1, \tag{9}$$

with $E_d(\Lambda) \equiv \sqrt{\pi/2}(d+1)(d+3)(\Lambda-1)^2/d$. For spherical particles the $\Phi\Psi^2$ dependence was derived in Ref. [32].

Let us now analyze the shape dependence of Eq. (7). The Λ dependence of $B_d(\Lambda)$ explains that rods ($\Lambda = 1$) cluster less than spheres ($\Lambda = 0$), consistent with the DNS results reported in Ref. [22]. But when gyrotaxis is weak, spheres are essentially randomly oriented, unlike neighbouring rods that are aligned by turbulent shears. In this limit motile rods must cluster more than spheres. This is demonstrated below, but it is not captured by Eqs. (7) and (9) which must fail for large Ψ because the limit $\Psi \to \infty$ is singular, and due to the occurrence of singularities in the dynamics of the gradients of $\boldsymbol{n}$ at large but finite values of Ψ (see Supplemental Material [31]). The first caveat also applies to Eqs. (5) and (6).

Fractal dimension.—DNS show [11] that the small-scale spatial patterns of motile gyrotactic organisms are fractal. This may substantially enhance their encounter rates [33]. We analyze the fractal patterns for finite but small Ku, in two dimensions. We expect qualitatively the same result in three dimensions. The fractal patterns are characterized by "Lyapunov exponents" λ_1 and λ_2

$$\lambda_1 \equiv \lim_{t\to\infty} t^{-1} \ln \frac{R(t)}{R(0)} \quad \text{and} \quad \lambda_1 + \lambda_2 \equiv \lim_{t\to\infty} t^{-1} \ln \frac{\mathcal{A}(t)}{\mathcal{A}(0)}. \tag{10}$$

These exponents quantify the expansion (contraction) rates of the distance $R(t)$ between two initially nearby particles, and of the area element $\mathcal{A}(t)$ spanned by the separation vectors between three nearby particles. The fractal Lyapunov dimension is defined by [24,34]

$$d_{\mathrm{L}} \equiv 1 - \lambda_1/\lambda_2, \tag{11}$$

assuming $\lambda_1 > 0$ and $\lambda_1 + \lambda_2 < 0$. When $d_{\mathrm{L}} < 2$ fractal clustering occurs. To evaluate d_{L} we use $\lambda_1 + \lambda_2 = \langle \boldsymbol{\nabla} \cdot \boldsymbol{v} \rangle_\infty$, Eq. (S32), and compute λ_1 to order Ku^4. The result is lengthy; in the Supplemental Material [31] we quote the result to order Ku^2, Eq. (S31). To this order it is independent of Ψ and Λ. For small values of Φ Eq. (S31) simplifies to $\lambda_1 \tau \sim \mathrm{Ku}^2(1 - 3\Phi^2)$ for $d = 2$. Together with (7) this implies $\Delta_{\mathrm{L}} \equiv d - d_{\mathrm{L}} \sim \Phi^2\Psi^2$ consistent with the results of Refs. [11,32] for spherical particles. Figure 2(a) shows the analytical result for d_{L} as a function of Φ. It is in good agreement with numerical simulations of the statistical model ($d = 2$) for $\mathrm{Ku} = 0.1$. We see that spherical organisms cluster more than rods. As explained above this is expected for strong gyrotaxis.

But when the effect of the gravitational torque is small then prolate organisms cluster more: in the absence of gyrotaxis, rotational symmetry ensures that active spherical particles remain uniformly distributed, but rodlike particles show fractal clustering. Panel (b) in Fig. 2 demonstrates this cross-over. It shows d_{L} for $\Phi = 1$, $\mathrm{Ku} = 1$ as a function

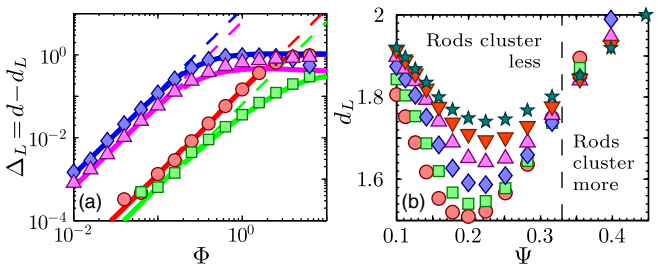

FIG. 2. (a) Fractal dimension deficit $\Delta_L \equiv d - d_{\mathrm{L}}$ for $d = 2$, $\mathrm{Ku} = 0.1$. Numerical simulations of statistical model for $\Psi = 0.1$, $\Lambda = 0$ (red filled circles), $\Psi = 1$, $\Lambda = 0$ (blue filled diamonds), $\Psi = 0.1$, $\Lambda = 1$ (light green filled squares), and $\Psi = 1$, $\Lambda = 1$ (pink filled triangles). Theory [Eqs. (11), (S31), and (S32)] including the Ku^4 contribution to Eq. (S31): solid lines. Asymptote $\propto (\Phi\Psi)^2$: dashed lines. (b) Numerical simulations, d_{L} for $d = 2$, $\Phi = 1$, $\mathrm{Ku} = 1$, $\Lambda = 0$ (red filled circles), 0.2 (light green filled squares), 0.4 (blue filled diamonds), 0.6 (pink filled triangles), 0.8 (red filled triangles), 1 (dark green filled stars).

of Ψ. We arrive at qualitatively similar conclusions by numerically computing the fractal correlation dimension d_2. But the numerical values found for d_2 differ from d_{L} This shows that the spatial distribution is multifractal [24].

Conclusions.—First, our statistical-model calculations explain how the dynamics of gyrotactic motile microorganisms depends on the dimensionless parameters of the problem: Λ (shape), Φ (swimming speed), and Ψ (reorientation time). Second, we find that the particles tend to preferentially sample positive values of A_{zz}, corresponding to sinks in the transversal flow, regardless of shape. We predict that this must also be observed in DNS; it is simply a consequence of the fact that gravity breaks the symmetry of the problem. At the same time our calculations show that spherical particles are more often found in regions where u_z is negative, explaining the behavior found in DNS [11]. But our calculations also predict that rodlike particles preferentially sample up-welling regions of homogeneous isotropic flows such as turbulence, provided that they swim fast enough. Third, we have analytically computed how the degree of small-scale spatial clustering depends on particle shape. This is important because small-scale fractal clustering may enhance particle-encounter rates. We find a transition that we predict to be observable in DNS as well: when gyrotaxis is strong (small Ψ) oblong particles cluster less than spherical ones, while at large Ψ the opposite is true.

Our calculations also show that singularities in the motion of nearby microorganisms occur, much like "caustics" for heavy particles in turbulence [35–38]. We predict that such singularities must also be observed in the DNS of gyrotactic microswimmers in turbulence. It is of interest to estimate how often the singularities occur because their effect may modify the predictions of phenomenological models for encounter rates [39].

The analytical results obtained in this Letter were derived for small Ku (or large Φ). But we have shown that our analytical results and the corresponding mechanisms qualitatively explain what is observed in DNS, and explain also the results of statistical-model simulations at large values of Ku. We find fairly good quantitative agreement between our statistical-model calculations and DNS results for fully developed turbulence. To achieve even better quantitative agreement with the DNS would require one to account for the universal non-Gaussian small-scale fluctuations of fully developed turbulence [26].

But the fluctuations of the unsteady ocean are neither fully developed turbulent, nor are they Gaussian. Therefore the fact that the much simpler Gaussian statistical model explains the dynamics observed in DNS of fully developed turbulence [11] shows that the analytical theory (and the underlying mechanisms) describe robust behavior, that must be taken into account in the analysis of patchiness and encounter rates of motile microorganisms in the ocean.

We thank the authors of Ref. [11] for permission to reproduce their data in Fig. 3(d). This work was supported by Vetenskapsrådet (VR), by a Linnaeus-grant from VR and Formas, by the Göran Gustafsson Foundation for Research in Natural Sciences and Medicine, and by the grant *Bottlenecks for particle growth in turbulent aerosols* from the Knut and Alice Wallenberg Foundation, Dnr. KAW 2014.0048. K. G. acknowledges partial funding from the European Research Council under the European Community's Seventh Framework Programme, ERC Grant Agreement No. 339032. The numerical computations used resources provided by the Centre for scientific and technical computing at Chalmers University of Technology in Gothenburg (Sweden) and the Swedish National Infrastructure for Computing.

[1] P. J. S. Franks and J. S. Jaffe, J. Mar. Syst. **69**, 254 (2008).
[2] C. L. Folt and C. W. Burns, Trends Ecol. Evol. **300**, 14 (1999).
[3] T. Kiørboe, *A Mechanistic Approach to Plankton Ecology* (Princeton University Press, Princeton, NJ, 2008).
[4] A. M. Roberts, J. Exp. Biol. **53**, 687 (1970).
[5] P. R. Jonsson, Mar. Ecol. Prog. Ser. **52**, 39 (1989).
[6] A. M. Roberts and F. M. Deacon, J. Fluid Mech. **452**, 405 (2002).
[7] J. O. Kessler, Nature (London) **313**, 218 (1985).
[8] W. M. Durham, J. O. Kessler, and R. Stocker, Science **323**, 1067 (2009).
[9] F. Santamaria, F. De Lillo, M. Cencini, and G. Boffetta, Phys. Fluids **26**, 111901 (2014).
[10] J. G. Mitchell, A. Okubo, and J. A. Fuhrmann, Limnol. Oceanogr. **35**, 123 (1990).
[11] W. M. Durham, E. Climent, M. Barry, F. de Lillo, G. Boffetta, M. Cencini, and R. Stocker, Nat. Commun. **4**, 2148 (2013).
[12] G. B. Jeffery, Proc. R. Soc. A **102**, 161 (1922).
[13] S. Parsa, E. Calzavarini, F. Toschi, and G. A. Voth, Phys. Rev. Lett. **109**, 134501 (2012).
[14] K. Gustavsson, J. Einarsson, and B. Mehlig, Phys. Rev. Lett. **112**, 014501 (2014).
[15] M. Byron, J. Einarsson, K. Gustavsson, G. A. Voth, B. Mehlig, and E. Variano Phys. Fluids **27**, 035101 (2015).
[16] M. Wilkinson, V. Bezuglyy, and B. Mehlig, Phys. Fluids **21**, 043304 (2009).
[17] V. Bezuglyy, B. Mehlig, and M. Wilkinson, Europhys. Lett. **89**, 34003 (2010).
[18] M. Wilkinson, V. Bezuglyy, and B. Mehlig, J. Fluid Mech. **667**, 158 (2011).
[19] C. Torney and Z. Neufeld, Phys. Rev. Lett. **99**, 078101 (2007).
[20] W. M. Durham, E. Climent, and R. Stocker, Phys. Rev. Lett. **106**, 238102 (2011).
[21] N. Khurana and N. T. Ouellette, Phys. Fluids **24**, 091902 (2012).
[22] C. Zhan, G. Sardina, E. Lushi, and L. Brandt, J. Fluid Mech. **739**, 22 (2014).
[23] F. De Lillo, M. Cencini, W. M. Durham, M. Barry, R. Stocker, E. Climent, and G. Boffetta, Phys. Rev. Lett. **112**, 044502 (2014).
[24] K. Gustavsson and B. Mehlig, arxiv:1412.4374.
[25] H. Pécseli, J. Trulsen, and Ø. Fiksen, Progr. Oceanogr. **101**, 14 (2012).
[26] J. Schumacher, J. Scheel, D. Krasnov, D. Donzis, V. Yakhot, and K. Sreenivasan, Proc. Natl. Acad. Sci. U.S.A. **111**, 10961 (2014).
[27] H. Yamazaki and K. D. Squires, Mar. Ecol. Prog. Ser. **144**, 299 (1996).
[28] A. E. Gargett, Annu. Rev. Fluid Mech. **21**, 419 (1989).
[29] K. Gustavsson and B. Mehlig, Europhys. Lett. **96**, 60012 (2011).
[30] K. Gustavsson, S. Vajedi, and B. Mehlig, Phys. Rev. Lett. **112**, 214501 (2014).
[31] See Supplemental Material at http://link.aps.org/supplemental/10.1103/PhysRevLett.116.108104 for details of the calculations, and for a Supplemental Figure.
[32] I. Fouxon and A. M. Leshansky, Phys. Rev. E **92**, 013017 (2015).
[33] B. Andersson, K. Gustavsson, B. Mehlig, and M. Wilkinson, Europhys. Lett. **80**, 69001 (2007).
[34] J. Kaplan and J. A. Yorke, Lect. Notes Math. **730**, 204 (1979).
[35] M. Wilkinson and B. Mehlig, Europhys. Lett. **71**, 186 (2005).
[36] G. Falkovich, A. Fouxon, and G. Stepanov, Nature (London) **419**, 151 (2002).
[37] K. Gustavsson, E. Meneguz, M. Reeks, and B. Mehlig, New J. Phys. **14**, 115017 (2012).
[38] K. Gustavsson and B. Mehlig, Phys. Rev. E **87**, 023016 (2013).
[39] B. J. Rothschild and T. R. Osborn, J. Plankton Res. **10**, 465 (1988).